Substrate positioning controls the partition between halogenation and hydroxylation in the aliphatic halogenase, SyrB2

Megan L. Matthews[a], Christopher S. Neumann[b], Linde A. Miles[c], Tyler L. Grove[a], Squire J. Booker[a,c], Carsten Krebs[a,c,1], Christopher T. Walsh[b,1], and J. Martin Bollinger, Jr.[a,c,1]

Departments of [a]Chemistry and [c]Biochemistry and Molecular Biology, Pennsylvania State University, University Park, PA 16802; and [b]Department of Biological Chemistry and Molecular Pharmacology, Harvard Medical School, Boston, MA 02115

Contributed by Christopher T. Walsh, August 27, 2009 (sent for review July 20, 2009)

The α-ketoglutarate-dependent hydroxylases and halogenases employ similar reaction mechanisms involving hydrogen-abstracting Fe(IV)-oxo (ferryl) intermediates. In the halogenases, the carboxylate residue from the His$_2$(Asp/Glu)$_1$"facial triad" of iron ligands found in the hydroxylases is replaced by alanine, and a halide ion (X^-) coordinates at the vacated site. Halogenation is thought to result from "rebound" of the halogen radical from the X-Fe(III)-OH intermediate produced by hydrogen ($H^\bullet$) abstraction to the substrate radical. The alternative decay pathway for the X-Fe(III)-OH intermediate, rebound of the hydroxyl radical to the substrate radical (as occurs in the hydroxylases), reportedly does not compete. Here we show for the halogenase SyrB2 that positioning of the alkyl group of the substrate away from the oxo/hydroxo ligand and closer to the halogen ligand sacrifices $H^\bullet$-abstraction proficiency for halogen-rebound selectivity. Upon replacement of L-Thr, the C4 amino acid tethered to the SyrB1 carrier protein in the native substrate, by the C5 amino acid L-norvaline, decay of the chloroferryl intermediate becomes 130× faster and the reaction outcome switches to primarily hydroxylation of C5, consistent with projection of the methyl group closer to the oxo/hydroxo by the longer side chain. Competing $H^\bullet$ abstraction from C4 results primarily in chlorination, as occurs at this site in the native substrate. Consequently, deuteration of C5, which slows attack at this site, switches both the regioselectivity from C5 to C4 and the chemoselectivity from hydroxylation to chlorination. Thus, substrate-intermediate disposition and the carboxylate → halide ligand swap combine to specify the halogenation outcome.

α-ketoglutarate | ferryl | hydroxylase | nonheme iron | radical rebound

The α-ketoglutarate-dependent oxygenases activate O_2 at mononuclear Fe(II) cofactors, cleave α-ketoglutarate (αKG) to CO_2 and succinate, and oxidize their substrates by two electrons (1–4). The most extensively studied members of the family are hydroxylases. A mechanism for the (pro)collagen-modifying prolyl-4-hydroxylase (P4H) originally proposed by Hanauske-Abel and Günzler (5) has accounted well for ensuing experimental data on multiple enzymes in the family. Its central tenets are the abstraction of a hydrogen atom ($H^\bullet$) from the substrate by an Fe(IV)-oxo (ferryl) complex (Scheme 1*A*, black arrows) and the subsequent "rebound" of the coordinated hydroxyl radical to the substrate radical (red arrows) (6). The most compelling evidence for this mechanism was provided by the detection and spectroscopic characterization of the ferryl intermediates in taurine:αKG dioxygenase (TauD) from *Escherichia coli* and a P4H from *Paramecium bursaria Chlorella virus* 1 (7, 8). The small Mössbauer isomer shifts (≈0.3 mm/s) and $S = 2$ electron-spin ground states of the freeze-trapped intermediates marked them as high-spin Fe(IV) complexes; the large substrate deuterium (D) kinetic isotope effects (KIEs) on their decay ($k_H/k_D \approx 50$) showed that they abstract hydrogen from the substrates (8, 9); and resonance Raman and X-ray absorption spectroscopic data on the TauD complex proved that it contains the ferryl unit (10, 11).

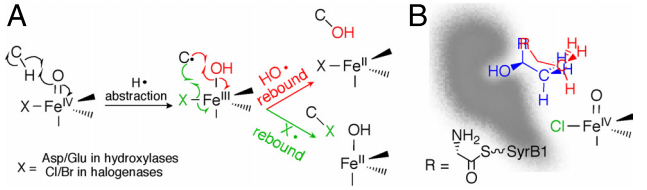

Scheme 1. Mechanistic and structural rationale for this study. (*A*) Proposed mechanisms for the last two steps in the reactions of αKG-dependent aliphatic hydroxylases (red) and halogenases (green). (*B*) Cartoon of active site with proposed positioning of **Thr** (blue) and **Aba** (red) substrates indicated by previously reported observations on the kinetics of chloroferryl intermediate decay (16).

Before the recent discovery of the aliphatic halogenases (12), a group of αKG-dependent oxygenases that synthesize precursors for assembly of halogen-containing natural products by nonribosomal peptide synthetases (NRPSs), iron coordination by a conserved 2-histidine-1-carboxylate "facial triad" had been considered a defining feature of the family (13). Sequence analysis and the crystal structure of SyrB2 (14), the halogenase that supplies the 4-chloro-L-threonine fragment incorporated into syringomycin E (a phytotoxin produced by *Pseudomonas syringae* B301D) (12), revealed that it lacks the carboxylate ligand, having an Ala residue where the contributing Asp or Glu would normally be found (Scheme 1*A*). The observation that a halide ion (X^-) coordinates to the Fe(II) cofactor at the vacated site suggested a related mechanism for the halogenase reaction involving abstraction of $H^\bullet$ from the substrate by the oxo group of a haloferryl intermediate and rebound of the coordinated halogen radical from the resultant X-Fe(III)–OH complex to the substrate radical (green arrows). Detection and characterization of the C–H-cleaving haloferryl states in two halogenases confirmed the central feature of this mechanism (15, 16).

The proposed halogenase mechanism raised two questions: does rebound of the coordinated hydroxyl radical equivalent (red arrows in Scheme 1*A*), the final step in the otherwise identical hydroxylase mechanism, compete with rebound of the halogen radical (green arrows), as has been shown to occur in analogous oxidation reactions mediated by inorganic transition metal complexes (17, 18)? If not, what factors ensure the strict halogen-rebound selectivity? The failure of attempts to detect the alcohol products of competing hydroxyl-radical rebound answered the first question in

Author contributions: M.L.M., T.L.G., C.K., and J.M.B. designed research; M.L.M., C.S.N., and L.A.M. performed research; M.L.M., C.S.N., T.L.G., S.J.B., and C.T.W. contributed new reagents/analytic tools; M.L.M., L.A.M., and J.M.B. analyzed data; and M.L.M., C.K., C.T.W., and J.M.B. wrote the paper.

The authors declare no conflict of interest.

[1]To whom correspondence may be addressed. E-mail: jmb21@psu.edu, christopher_walsh@hms.harvard.edu, or ckrebs@psu.edu.

This article contains supporting information online at www.pnas.org/cgi/content/full/0909649106/DCSupplemental.

the negative (12, 14). The report that the A118E variant of SyrB2, with the carboxylate ligand of the facial triad restored, is not an efficient hydroxylase (14) suggested that additional adaptations, beyond the manifest carboxylate → halide iron ligand swap, must have accrued during the evolutionary divergence of the halogenases and hydroxylases to distinguish their outcomes.

Our recent findings (15, 16) that the chloroferryl complexes in CytC3 and SyrB2 abstract H• from their substrates very sluggishly ($\approx 10^{-1}$ s^{-1} at 5 °C) in comparison with the corresponding steps in the two hydroxylases [$\approx 10^{1}$ to 10^{2} s^{-1} (7, 8)] and that modification of the native SyrB2 substrate (the SyrB1 carrier protein tethered on its phosphopantetheine cofactor by L-Thr; hereafter denoted **Thr**) by removal of the β-hydroxyl group (giving L-2-aminobutyryl-SyrB1; hereafter **Aba**) accelerates H• abstraction in SyrB2 by more than 10-fold (16) suggested to us that the halogenases might bind their substrates so as to position the H•-donating carbons away from the oxo/hydroxo ligands and nearer to the halogens, thereby sacrificing H•-abstraction proficiency for rebound selectivity. According to this hypothesis, the faster H• abstraction with **Aba**, having stronger scissile C–H bonds than the native **Thr** [deduced by comparison of homolytic bond dissociation energies (BDEs) of relevant models (19)], could reflect (*i*) the loss of the β-OH group that would otherwise anchor the target methyl in this halogen-proximal position and (*ii*) the consequent closer approach of the methyl group to the oxo (Scheme 1*B*). This hypothesis implies that side-chain modifications pushing the potential H• donors even closer to the chloroferryl oxo group might both further accelerate H• abstraction and permit hydroxylation.

In this study, we have confirmed that substrate positioning is of primary importance in determining both H•-abstraction proficiency and Cl•/HO• radical-rebound selectivity. Mass spectrometric analysis of the **Aba** reaction products shows that the more rapid H• abstraction with this substrate is associated with a marked increase in hydroxylation in comparison to the **Thr** reaction. More compellingly, SyrB1 presenting covalently tethered L-norvaline (**Nva**), with an additional methylene unit in the amino acid side chain intended to project a H• donor even closer to the oxo group, shows three remarkable properties upon incubation with SyrB2: (*i*) it undergoes H• abstraction 10× faster than **Aba** and 130× faster than **Thr**; (*ii*) it is modified primarily at its C5 methyl group, almost exclusively by hydroxylation; and (*iii*) it undergoes primarily chlorination at C4 when chemistry is redirected there by deuterium substitution at C5. Combined with the confirmation by ^{18}O-labeling experiments that the hydroxyamino acid products form by an O-atom insertion mechanism, the results show that the halogenase is inherently competent as a hydroxylase but avoids this outcome by properly positioning its substrate's H•-donating C4 methyl to favor capture of the halogen in the radical rebound step.

Results

Definition of the Kinetics of the SyrB2 Reaction with Nva Substrate. To test the hypothesis that an additional methylene unit in the amino acid side chain might project a H•-donor closer to the chloroferryl intermediate and thereby accelerate H• abstraction, the reactions of SyrB2 in the presence of SyrB1 substrate presenting either unlabeled L-norvaline (**Nva**) or L-[4,4,5,5,5-$^{2}H_5$]norvaline (**4,5-d_5-Nva**) were examined in stopped-flow absorption (SF-abs) experiments. The absorbance at 320 nm, used in previous studies to track the H•-abstracting (halo)ferryl intermediates (7, 8, 15, 16), rises and falls in both reactions (Fig. 1, squares and circles), indicative of accumulation of the chloroferryl state. Combined analysis of the two traces indicates that the small amplitude of the transient in the **Nva** reaction (squares) arises from a combination of the slower formation ($k_{form} = 0.8 \pm 0.2$ s^{-1} at 5 °C with 0.9 mM O_2) and faster decay ($k_{decay} = 9.5 \pm 1.0$ s^{-1}) of the intermediate than has been observed for other substrates. This kinetic situation is accurately diagnosed by comparison to the trace for the **4,5-d_5-Nva** substrate (circles), which has a much larger amplitude as a consequence of the drastic slowing of decay of the intermediate ($k_{decay} = 0.17 \pm 0.02$ s^{-1}) by the large D-KIE (56 ± 10). The modest value of k_{form} indicates that, not surprisingly, the **Nva** substrate is less effective at conformationally triggering the halogenase to react with O_2 than are other nonnative substrates that differ less profoundly from the native **Thr** [e.g., **Thr** gives $k_{form} = 48 \pm 4$ s^{-1} and **Aba** gives $k_{form} = 8 \pm 1$ s^{-1} under identical reaction conditions (16)]. More importantly, the fact that the value of k_{decay} for the protium-containing **Nva** is 10× that previously observed for **Aba** and 130× that for the native **Thr** is consistent with the hypothesis regarding the role of positioning in halogenase chemoselectivity.

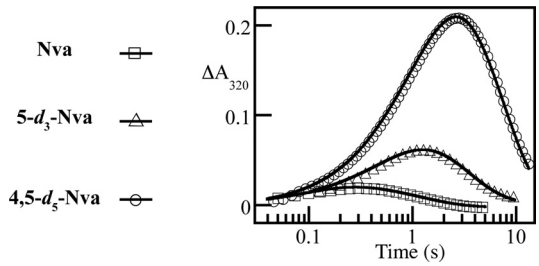

Fig. 1. Absorbance (320 nm) versus time traces obtained after O_2-saturated reaction buffer (20 mM Hepes, pH 7.5) was mixed with an equal volume of an O_2-free solution containing SyrB2 (0.38–0.60 mM), Fe(II) (0.30 mM), αKG (10 mM), Cl^- (100 mM), and the indicated substrate [≥3 equiv or 0.90 mM; **Nva** (squares), **5-d_3-Nva** (triangles), and **4,5-d_5-Nva** (circles)]. Solid lines are fits to the data as previously described (16), giving parameters quoted in the text.

Determination of the Efficiencies of Coupling of αKG and Substrate Oxidation. The general αKG-dependent-oxygenase mechanism theoretically permits one substrate molecule to be oxidized per molecule of αKG decarboxylated, but this "coupling ratio" can be diminished to less than unity by unproductive pathways, such as one might expect to become engaged in reactions with profoundly nonnative substrates. The coupling ratios for the three pantetheinyl tethered substrates, **Thr**, **Aba**, and **Nva**, were determined by MS analysis (described in *SI Text*) of SyrB2 reactions carried out with varying and limiting αKG and excess substrate and O_2. Representative, reconstructed mass spectra are shown in Fig. 2. For each of the three substrates, an increase in the αKG/substrate ratio results in the expected diminution of the MS peak for the unlabeled substrate (blue bars in the first four rows on right-hand axes of Fig. 2 *A–C*) relative to that for the deuterium-labeled standard (black bars). The relative intensities of blue and black bars exhibit the expected reversal in the experiments for which the deuterium-labeled amino acids were instead used in the reactions and the unlabeled compounds as standards (fifth rows in right-hand axes of Fig. 2 *A–C*). From the relative intensities of blue and black bars in rows 1–4 and the known initial concentrations of the unlabeled substrates, the concentration of substrate consumed at each αKG/substrate ratio was calculated for each substrate. The slopes of the three lines in the resulting two-dimensional plots (Fig. S1) are the coupling ratios. Surprisingly, this ratio is only ≈0.5 (0.55 ± 0.07) for the native **Thr** substrate (red circles) but is closer to unity (0.97 ± 0.10 for **Aba** and 0.75 ± 0.10 for **Nva**) for the two nonnative substrates (blue and black circles). Thus, the nonnative substrates are consumed even more efficiently than the native **Thr**, giving confidence that the products detected reflect major reaction pathways.

Mass Spectrometric Characterization of Reaction Products. Whereas rigorous quantitation of the reaction products could not be performed because of the lack of access to isotopic product-SyrB1 species to include as recovery and MS-intensity standards, the reconstructed mass spectra in Fig. 2 still reveal striking trends in product distribution. For the native **Thr** (Fig. 2*A*), peaks corre-

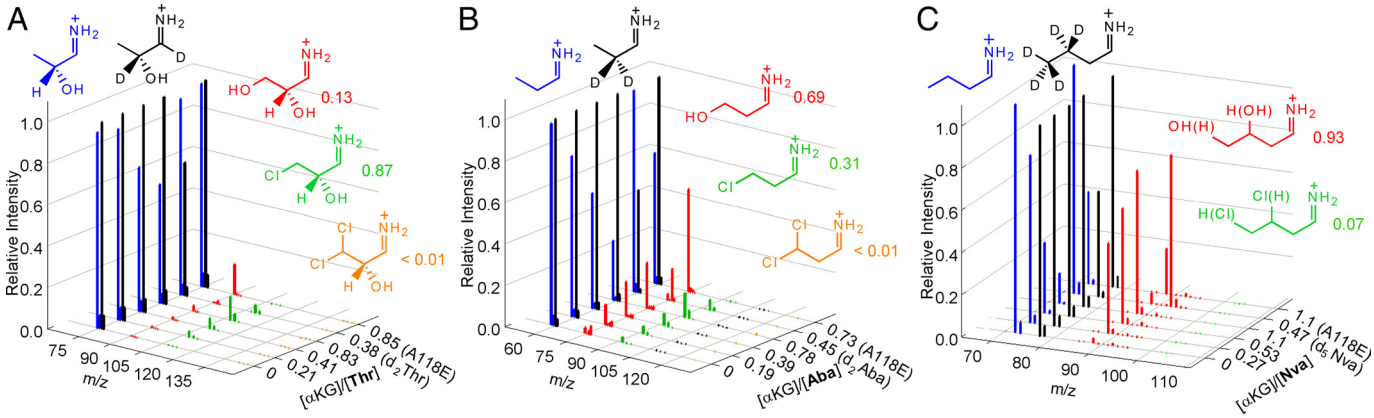

Fig. 2. Representative, reconstructed mass spectra depicting the relative intensities of substrate and product iminium daughter ions obtained with **Thr** (*A*), **Aba** (*B*), and **Nva** (*C*) under the conditions defined along the *z* axis: rows 1–4, αKG dependence for the reaction with unlabeled substrate (concentrations of αKG displayed as equivalents relative to the substrate concentration); row 5, sample in which the unlabeled substrate was used as the standard and the deuterated substrate (**2,3-d_2-Thr**, **3-d_2-Aba**, or **4,5-d_5-Nva**) in the reaction; and row 6, reaction with the SyrB2-A118E variant. Color-coded icons show the structure of each daughter ion of the substrate (in blue), the labeled standard (in black), and the major products (hydroxylated in red and chlorinated in green) that could be unequivocally detected. The *m/z* values for each hydroxamate parent ion → iminium daughter ion transition are defined in Tables S1–S3. The fraction of the total peak intensity attributable to products that is contributed by each daughter ion is displayed below the appropriate icon. Note that these are not mole fractions. Note also that in *C*, the regiochemistry of the hydroxyl- and chloro-Nva products cannot be determined. Sample preparation and analysis are described in *SI Text*.

sponding to the iminium fragment ion of the monochlorination product at m/z = 108.0 (^{35}Cl) and m/z = 110.0 (^{37}Cl) have the proper isotopic ratio of approximately 3:1 and increase in intensity proportionally to αKG/**Thr** (green bars, rows 1–4 on the right-hand axis). Peaks at m/z = 142.0 and m/z = 144.0 for the dichlorination product are essentially absent. The peak at m/z = 90.1, expected to result from hydroxylation, is just barely detectable (red bars), in agreement with previous reports that the halogenases are highly selective against hydroxylation (12, 14). The weak intensity does, however, increase with increasing αKG/**Thr** (compare rows 1–4), implying that hydroxylation of the native substrate may compete to a minor extent. Use of **2,3-d_2-Thr** as substrate shifts the peaks for the chloro and hydroxy products by the expected two mass units (row 5 on right-hand axis). Use of the A118E variant of SyrB2, previously shown to "restore" the carboxylate ligand of the facial triad, but to yield inactive enzyme (14), essentially abolishes chlorination (row 6). This result is consistent with the expectation that the presence of the E118 carboxylate should prevent Cl^- coordination to the Fe(II) cofactor and thereby preclude halogen-radical rebound. Also consistent with previous reports, the variant does not appear to efficiently hydroxylate the native substrate (14). However, the intensity of the peak for the hydroxylated product is significantly (≈7-fold) greater for variant than for wild-type SyrB2, confirming the expectation that the mere presence of the Cl ligand in the chloroferryl state contributes to the suppression of substrate hydroxylation by the halogenases.

The reconstructed spectra for the reaction with **Aba** reveal notable differences (Fig. 2*B*). As stated, the steeper decline of the peak for unlabeled substrate (blue bars) with increasing αKG/**Aba** reflects an increased coupling ratio. More importantly, in addition to the peaks for the monochlorinated product (green), which increase in intensity with the expected dependence on αKG/**Aba** (rows 1–4 on right-hand axis) and shift appropriately when **3-d_2-Aba** is instead used in the reaction (row 5), prominent peaks (red) for the hydroxylated product at m/z = 74.1 increase with αKG/**Aba** (rows 1–4) and shift as expected to m/z = 76.1 for **3-d_2-Aba** (row 5). Use of the A118E variant eliminates the peaks for the chlorinated product and enhances that for the hydroxylated product (row 6), as seen with the native substrate.

For the **Nva** substrate (Fig. 2*C*), the peaks for the monochlorinated product (green) are much weaker, and that for the hydroxylated product (red) is much stronger than for **Aba** (rows 1–4). In this case, use of the A118E variant actually diminishes the intensity of this peak (row 6), suggesting that the substitution diminishes the coupling ratio in the predominant hydroxylation activity of SyrB2 toward **Nva**.

Hydroxylation of Aba and Nva Proceeds by O-Atom Insertion. To rule out the possibility that the hydroxylated products observed in the **Aba** and **Nva** reactions result from hydrolysis of the initial chlorinated products, these reactions were carried out in the presence of $^{18}O_2$ gas (95–98 atom % ^{18}O). Controls were performed in which atmospheric O_2 (99.8% ^{16}O) was instead used. Comparison of the reconstructed mass spectra from the **Nva** $^{18}O_2$ reaction and the $^{16}O_2$ control (Fig. S2) proves that the hydroxylated product (hydroxyamino acid) is indeed formed by an authentic hydroxylation (O-atom-insertion) mechanism. The spectrum of the $^{18}O_2$ sample (row 3) has a prominent peak at m/z = 90.1, corresponding to addition of 18 atomic mass units to the substrate-derived fragment, in addition to a less intense peak at m/z = 88.1 for the ^{16}O-modified species (relative intensity 0.67:0.33). The spectrum of the control sample (row 4) essentially lacks the m/z = 90.1 peak. With **4,5-d_5-Nva**, having deuteria at both potentially H•/D•-donating sites, the ratio of intensities of the ^{18}O- and ^{16}O-product peaks at m/z = 94.1 and 92.1 changes considerably to 0.1:0.9 (row 5), indicative of greater exchange of the ^{18}O in the chloroferryl complex with $H_2{}^{16}O$ solvent as a consequence of the slowing of H•/D• abstraction from 9.5 s^{-1} to 0.17 s^{-1}. Although the ^{18}O:^{16}O ratio in the hydroxylated product from the **Aba** reaction (row 1) is even less (0.08:0.92), the ^{18}O-associated peak is still sufficiently (8-fold) more intense than the corresponding peak in the control reaction (row 2) to prove that **Aba** hydroxylation also occurs by an O-atom-insertion mechanism. Thus, SyrB2 can, in fact, default to become an authentic hydroxylase when challenged with the nonnative substrates.

Assessment of Regiochemistry by Use of Site-Specifically Deuterated Nva Residues. The C4 methyl of the tethered Thr is the site of chlorination in the native **Thr** substrate (12). By contrast, **Nva** was selected with the intent of projecting its C5 methyl group closer to the oxo of the chloroferryl intermediate; hydroxylation at C5 is therefore anticipated. [Previous results from the reaction with **Ala** showing (*i*) stability of the chloroferryl intermediate for tens of minutes, (*ii*) its decay to Fe(III) products, and (*iii*) no observable D-KIE on chloroferryl decay with the use of **3-d_3-Ala** establish that

BIOCHEMISTRY

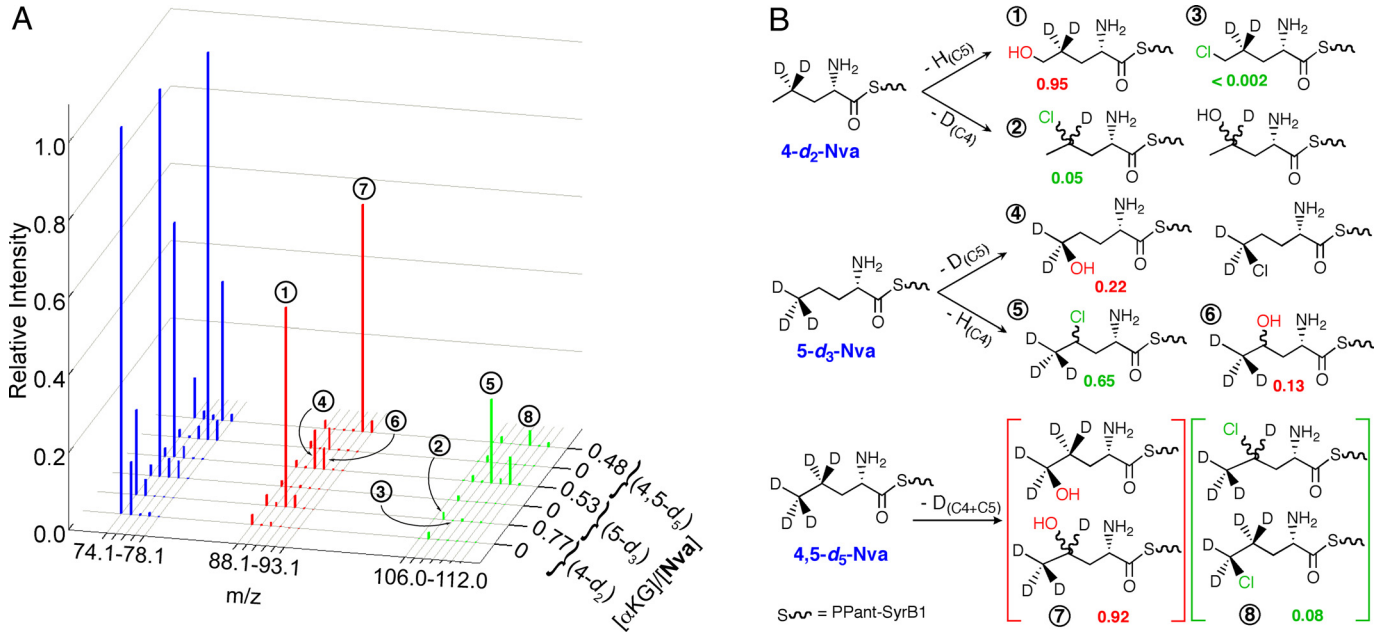

Fig. 3. MS analysis of SyrB2 reactions with deuterated **Nva** substrates. (*A*) Representative, reconstructed mass spectra depicting the relative intensities of substrate and product daughter ions obtained with **4-d_2-Nva** (4-d_2), **5-d_3-Nva** (5-d_3), and **4,5-d_5-Nva** (4,5-d_5) substrates in the absence and presence of αKG (equivalents of αKG relative to the substrate concentration are shown along the *z* axis). For each reaction, unlabeled **Nva** was used as the normalization standard, but its peak is not shown for esthetic purposes. Peaks correspond to the iminium daughter ions of each labeled substrate (blue), hydroxylated product (red), and chlorinated product (green). (*B*) Interpretation of the MS data in *A* in terms of relative intensities of peaks (labeled ①–⑧) that correspond to the reaction products for each substrate. Site of modification (chlorination or hydroxylation) in the daughter ions was inferred from whether H (1 atomic mass unit) or D (2 atomic mass units) was lost from the specifically deuterated **Nva** substrate. The *m/z* values for each hydroxamate parent ion → iminium daughter ion fragmentation are defined in Table S3. As for the reaction with unlabeled **Nva** in Fig. 1*C*, regiochemistry of the products in the **4,5-d_5-Nva** reaction cannot be determined (C4 and C5 hydroxylated and chlorinated products shown in brackets). Sample preparation and analysis are described in *SI Text*.

neither C2 nor C3 can donate H• with appreciable proficiency (16).] To test this prediction, site-specifically deuterated **Nva** substrates, presenting [5,5,5-$^2H_3$]Nva (**5-d_3-Nva**) and [4,4-$^2H_2$]Nva (**4-d_2-Nva**), were constructed. SF-abs experiments revealed that the formation and decay kinetics of the chloroferryl intermediate in the **4-d_2-Nva** reaction are indistinguishable from those in the reaction with protium substrate (Fig. S3). By contrast, the chloroferryl state in the reaction with **5-d_3-Nva** (Fig. 1, triangles) decays at approximately 1.5 s^{-1}, intermediate between the decay rate constants for **Nva** and **4,5-d_5-Nva**. The absence of a detectable D-KIE for **4-d_2-Nva** and intermediate D-KIE for **5-d_3-Nva** suggest that the C5 methyl group is the primary site of H• abstraction but the C4 methylene can donate H• less efficiently.

MS analysis of the products of these reactions confirms the interpretation of the SF-abs data and provides much deeper insight. In the reconstructed spectra from the **4-d_2-Nva** reaction (Fig. 3*A*, row 2 of right-hand axis), the prominent peak at *m/z* = 90.1 (labeled ① in Fig. 3) corresponds to addition of 16 atomic mass units to the substrate-derived fragment, which implies removal of protium, necessarily from C5, during hydroxylation. The peak at *m/z* = 89.1, which would reflect hydroxylation with loss of one of the two deuteria from C4, is not significantly enhanced relative to the corresponding peak in the spectrum of the control reaction lacking αKG (row 1). Remarkably, weak peaks at *m/z* = 107.0 (②) and 109.0 suggest that the chlorination product forms by removal of deuterium from C4, whereas the *m/z* = 108.0 (③) and 110.0 peaks expected for chlorination at C5 (with loss of protium) are much weaker still (row 2).

The data for the **5-d_3-Nva** reaction (row 4) are even more striking. Peaks at *m/z* = 90.1 (④) and 91.1 (⑥), corresponding to hydroxylation at C5 and C4, respectively, are both readily detected, with the former being the more intense. This observation indicates that hydroxylation at C4 becomes competitive when reaction at C5 is slowed by deuterium substitution. Even with the rate reduction from the large D-KIE, C5 is still the preferred target with respect to hydroxylation. By contrast, the peaks at *m/z* = 109.0 (⑤) and 111.0, corresponding to loss of protium from C4 during chlorination, are by far the most intense in the spectrum, and peaks at *m/z* = 108.0 and 110.0 for loss of deuterium from the C^5D_3 group during chlorination are essentially absent. Thus, the site giving the more rapid H• abstraction (C5) preferentially undergoes hydroxylation, whereas the site giving the less rapid H• abstraction (C4) preferentially undergoes chlorination. Consequently, the large D-KIE disfavoring C5 as donor in **5-d_3-Nva** switches not only the (overall) preferred site of H• abstraction to C4 but also the preferred outcome from hydroxylation to chlorination. Deuterium substitution at both C4 and C5 (**4,5-d_5-Nva**) makes hydroxylation again predominant (row 6, peak ⑦). Fig. 3*B* summarizes the outcomes of the reactions with the deuterium-labeled **Nva** substrates. It is important to note that the numbers given in the figure are not mole fractions but rather relative MS intensities from Fig. 3*A*.

Discussion

Since the relatively recent discovery of the mononuclear, nonheme iron halogenases (12), all attempts to detect products of hydroxyl-radical rebound occurring in competition with the preferred halogen-radical rebound have been unsuccessful (12, 14). At least five distinct hypotheses have been advanced to explain their (apparently) strict radical-rebound selectivity. First, it was argued on the basis of the rank order of reduction potentials (Br• < Cl• < HO•) that halogen-radical rebound might be favored simply by inherent reactivity (15). Studies on a selectively chlorinating inorganic iron complex (20) were cited as precedent for this possibility. Second, the X-ray crystallographic study on SyrB2 cited substrate positioning during the reaction as a probable contributing factor, although aminoacyl-SyrB1 substrate was not present in the crystal and

therefore not visualized (14). Third, when Mössbauer spectra of the C–H-cleaving haloferryl states in CytC3 and SyrB2 suggested the presence of two rapidly interconverting coordination isomers, a complexity not observed for the hydroxylases (15, 16), it was speculated that analogous dynamics in the X-Fe(III)-OH "rebound intermediate" might promote halogen radical rebound. Fourth, a computational study suggested that the CO_2 produced from αKG in formation of the haloferryl state carries the hydroxyl group away from the rebound intermediate in the form of bicarbonate, leaving only the halogen to be transferred to the substrate radical (21). Finally, a more recent computational study suggested that protonation of the hydroxyl group in the rebound intermediate, converting it to water, impedes rebound of the oxygen ligand (22).

A synthesis of published structural and kinetic data suggested to us that substrate positioning could be the primary chemoselectivity determinant in SyrB2. First, the A118E substitution, anticipated to "restore" the carboxylate ligand of the hydroxylase facial triad and thereby to displace the coordinated halide, was shown, as expected, to abrogate chlorination activity but, more surprisingly, not to confer hydroxylation activity (14). This result weighed against inherent Cl$^\bullet$/HO$^\bullet$ rebound reactivity as the primary chemoselectivity determinant: in this case, removal of the more rapidly rebounding halogen radical equivalent ought to have allowed the less reactive hydroxyl radical equivalent to rebound instead. Second, comparison of the rate constants for H$^\bullet$ abstraction by the chloroferryl intermediates in CytC3 and SyrB2 [$\approx 10^{-1}$ s^{-1} (15, 16)] and the ferryl complexes in TauD and P4H [$\approx 10^{1}$ to 10^{2} s^{-1} (7, 8)] hinted that the halogenases did not evolve primarily for maximum proficiency in this step. Whereas the unknown effect of halogen coordination on ferryl reactivity initially made direct comparison of the halogenase and hydroxylase rate constants perilous, the subsequent observations with **Aba** confirmed that the SyrB2 chloroferryl intermediate is, in fact, sufficiently potent to abstract H$^\bullet$ at least 10-fold more rapidly than it does from the native substrate (16), even from a C–H bond stronger than that in the native substrate. The reversal from the expected rank order of H$^\bullet$-abstraction rate constants for **Thr** and **Aba** showed that some other factor overrides the influence of C–H BDE. Third, the large D-KIEs observed in the halogenase reactions (15, 16) had established that H$^\bullet$ abstraction involves quantum mechanical tunneling. Theoretical studies indicate that hydrogen-tunneling reactions are exquisitely sensitive to donor–acceptor distance (23). Although the lack of a structure of any halogenase bound to its aminoacyl-carrier protein substrate has thus far precluded direct assessment of the disposition of the substrate side chain relative to the iron cofactor, it seemed likely that the factor overriding the influence of BDE might be proximity of the donor to the oxo acceptor. Accordingly, removal of a binding determinant (the 3-OH group of Thr) helping to anchor the H$^\bullet$-donating C4 methyl might (in **Aba**) allow it to flex closer to the oxo (Scheme 1*B*), making H$^\bullet$ abstraction faster (16). But closer donor–acceptor proximity in the chloroferryl state might necessarily be accompanied by closer approach of the substrate radical to the hydroxyl of the Cl–Fe(III)–OH in the rebound state, favoring hydroxylation. The analysis thus provided a hypothetical, comprehensive explanation for the meager H$^\bullet$-abstraction rate constants for the halogenases acting on their native substrates, the enhancement thereof by modification of the SyrB2 substrate, and the high chemoselectivity for halogenation over hydroxylation. More importantly, it suggested a straightforward test: to insert an additional methylene unit with the expectations of projecting the H$^\bullet$-donating methyl even closer to the oxo/hydroxo, further accelerating H$^\bullet$ abstraction, and promoting hydroxylation.

The verification of these predictions is strong evidence for the primacy of substrate positioning in determining halogenase chemoselectivity. The correlation between H$^\bullet$-abstraction rate constant and extent of hydroxylation across the series **Thr**, **Aba**, and **Nva** is in complete accordance with the expectation that the rates of both H$^\bullet$ abstraction and HO$^\bullet$ rebound are controlled by proximity of the substrate carbon to the Fe-coordinated oxygen (oxo or hydroxo) in the relevant intermediate. The results with **Nva** and its specifically deuterated forms are even more compelling evidence for the importance of substrate positioning and can be understood according to Scheme 2. We assume that H$^\bullet$ abstraction is slow compared with the ensuing rebound of Cl$^\bullet$ or HO$^\bullet$ (in competition), which render H$^\bullet$ abstraction also effectively irreversible. These assumptions are consistent with the large D-KIE on decay of the chloroferryl state, which would tend to be diminished from the intrinsic value for H$^\bullet$ abstraction by significant reversibility in this step, the fact that the alkyl-radical-containing rebound state has never been observed to accumulate in a hydroxylase or halogenase, and the known rapidity of capture of carbon radicals by oxygen ligands in inorganic chromium and manganese complexes (24, 25). The **Nva** reaction has two partition points. The first, the H$^\bullet$-abstraction step, determines the regioselectivity (C4 versus C5, horizontal arrows), and the second, the radical-rebound step, determines the chemoselectivity (halogenation vs. hydroxylation, vertical arrows). The kinetic data permit estimation of a set of rate constants for H$^\bullet$/D$^\bullet$ abstraction from C4 (light blue arrow, left side) and C5 (dark blue arrow, right side). The rate constants for decay of the chloroferryl intermediate determined in the SF-abs experiments (9.5 s^{-1} for **Nva**, 1.5 s^{-1} for **5-*d*$_3$-Nva**, and 0.17 s^{-1} for **4,5-*d*$_5$-Nva**) represent the sum of the rate constants for the individual H$^\bullet$-abstraction steps. Abstraction from C5 is favored by approximately 6-fold when both positions have protia, becomes disfavored by approximately 10-fold when only C5 is deuterated, and is again favored when both C4 and C5 are deuterated. The magnitude of the effect of deuteration only of C4 is the most difficult to assess, because the small difference between the large rate constants for chloroferryl decay with **4-*d*$_2$-Nva** and **Nva** cannot reliably be quantified. It is reasonable to assume that all three hydrons on the C5 methyl group are equally accessible to the oxo as a consequence of rapid rotation about the C4–C5 bond. By contrast, it is expected that only one of the two diastereotopic C4 hydrons will project toward the oxo. Thus, a statistical factor of 3 favoring H$^\bullet$ abstraction from C5 is perhaps anticipated. However, the C–H(D) bonds to C5 are expected to be approximately 3 kcal/mol stronger than those to C4 (19), which should favor abstraction from C4. The fact that C5 is the preferred site by twice the statistical factor of 3 again shows that some other factor (proximity to the oxo) overrides the expected influence of BDE, in this case in an intramolecular sense.

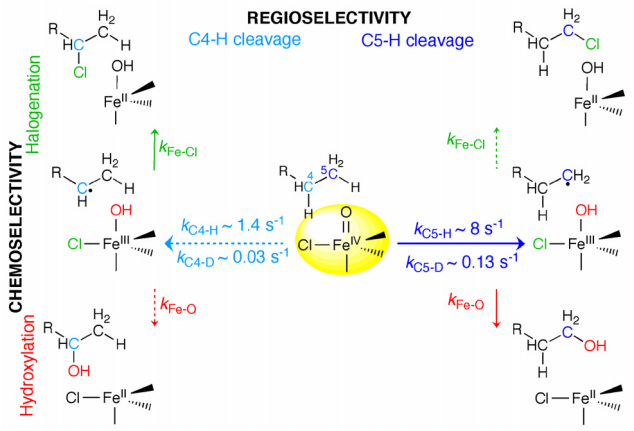

Scheme 2. Interpretation of the kinetic and mass spectral data with protium- and deuterium-containing **Nva** substrates. The rate constants for H$^\bullet$ abstraction are only estimates that are consistent with the observed rate constants for decay of the chloroferryl state in the presence of the various substrates. In particular, the rate constant for D$^\bullet$ abstraction from C4 is very poorly determined and could differ by as much as a factor of 3.

It is impossible to estimate rate constants for the individual radical-rebound steps to C4 and C5, both because these steps are obscured by unfavorable kinetics (slower formation and faster decay of the rebound state) and because the MS data do not provide for rigorous quantitation of the chlorinated and hydroxylated products. Nevertheless, qualitative trends are clear. After $H^{\bullet}$ abstraction from C5, rebound of the hydroxyl radical (red downward arrow) is vastly predominant over rebound of the chlorine radical (green upward arrow). In the **4-d_2-Nva** reaction, the intensity of the peak for chlorination with loss of protium is $<0.002\times$ that of the major peak for hydroxylation and near the lower limit of detection. Indeed, the major chlorinated species has lost deuterium, implying that chlorination occurs predominantly at C4, in opposition to the large intramolecular selection effect against C4–D cleavage. In the **5-d_3-Nva** reaction, the large selection effect against C5–D cleavage redirects toward $H^{\bullet}$ abstraction from C4. Both C4 hydroxylation and C4 chlorination are readily detected, implying that the two radical-rebound steps are competitive when the radical is generated at C4. Nevertheless, chlorine radical rebound is apparently faster, as it is to C4 of both **Aba** and, more stringently, the native **Thr**. Again, $D^{\bullet}$ abstraction from **5-d_3-Nva**, the minor pathway in this case, leads almost exclusively to hydroxylation: peaks for chlorination with loss of deuterium are not sufficiently intense nor of the proper ($^{35}Cl/^{37}Cl$) isotopic ratio to establish that any chlorination of C5 occurs.

The data thus establish a tight correlation, in both inter- and intramolecular contexts, between rate of $H^{\bullet}$ abstraction and proficiency of hydroxyl-radical rebound. In the **Nva** substrate, which is capable of both radical-rebound steps, C4 behaves much like C4 of **Aba**, supporting $H^{\bullet}$ abstraction at approximately 1.4 s^{-1} [compared with 0.9 s^{-1} (16) or a statistically corrected value of 0.3 s^{-1} for the Aba C4 methyl] and competitive rebound of the chlorine and hydroxyl radical equivalents. Note that the rank order of rate constants for $H^{\bullet}$ abstraction from the C4 methylene of **Nva** and C4 methyl of **Aba** parallels that expected from the estimated BDEs. Presumably, similar positioning of the C4 carbons in **Aba** and **Nva** removes the dominant effect and allows the more subtle influence of C–H BDE to be expressed. By contrast, the rate constant of 8 s^{-1} (or 2.7 s^{-1}) for $H^{\bullet}$ abstraction from the C5 methyl of **Nva** is at least twice that for cleavage of the weaker C4–H bond and almost $10\times$ that for cleavage of the approximately energetically equivalent C4–H of **Aba**. Correspondingly, rebound of the hydroxyl radical to the C5 substrate radical is strongly favored over rebound of the chlorine radical. The simplest and most likely explanation is that C5 approaches the oxo more closely than C4, enhancing $H^{\bullet}$ abstraction but subsequently thwarting chlorination. The analysis implies that a key principle underlying the design of the SyrB2 active site is binding of the carrier protein so as to position the scissile C–H bond away from the oxo and closer to the halogen, sacrificing proficiency in $H^{\bullet}$ abstraction to achieve selectivity in radical rebound. It seems likely, but remains to be established, that other halogenases have evolved similarly.

Experimental Procedures

Chemicals. L-norvaline (Nva) and hydroxylamine were purchased from Sigma–Aldrich. 2,3-d_2-Thr, 3-d_2-Aba, and 4,5-d_5-Nva were purchased from C/D/N. $^{18}O_2$ (95–98 atom %) was purchased from Icon Isotopes. 5-d_3-Nva and 4-d_2-Nva were synthesized by a published procedure (15), with the modifications described in *SI Text*. All other chemicals were obtained from sources previously noted (16).

Protein Preparation, Substrate Assembly, SF-abs Experiments, and Kinetic Analysis. These steps were performed as previously described (16).

Preparation of Samples and Analysis Thereof by Liquid Chromatography/Mass Spectrometry (LCMS). LCMS experiments were carried out on Agilent 1200 series LC system coupled to a triple quadrupole mass spectrometer (Agilent 6410 QQQ LC/MS; Agilent Technologies). Details of sample preparation, MS acquisition, and data analysis are given in *SI Text*.

ACKNOWLEDGMENTS. This work was supported by grants from the National Institutes of Health (GM-20011 and GM-49338 to C.T.W. and GM-69657 to J.M.B. and C.K.) and the National Science Foundation (MCB-642058 and CHE-724084 to J.M.B. and C.K.).

1. Solomon EI, et al. (2000) Geometric and electronic structure/function correlations in non-heme iron enzymes. *Chem Rev* 100:235–349.
2. Costas M, Mehn MP, Jensen MP, Que L, Jr (2004) Dioxygen activation at mononuclear nonheme iron active sites: Enzymes, models, and intermediates. *Chem Rev* 104:939–986.
3. Hausinger RP (2004) Fe(II)/α-ketoglutarate-dependent hydroxylases and related enzymes. *Crit Rev Biochem Mol Biol* 39:21–68.
4. Krebs C, Galonić Fujimori D, Walsh CT, Bollinger JM, Jr (2007) Non-heme Fe(IV)-oxo intermediates. *Acc Chem Res* 40:484–492.
5. Hanauske-Abel HM, Günzler V (1982) A stereochemical concept for the catalytic mechanism of prolylhydroxylase. Applicability to classification and design of inhibitors. *J Theor Biol* 94:421–455.
6. Groves JT (1985) Key elements of the chemistry of cytochrome P-450. The oxygen rebound mechanism. *J Chem Ed* 62:928–931.
7. Price JC, Barr EW, Tirupati B, Bollinger JM, Jr, Krebs C (2003) The first direct characterization of a high-valent iron intermediate in the reaction of an α-ketoglutarate-dependent dioxygenase: A high-spin Fe(IV) complex in taurine/α-ketoglutarate dioxygenase (TauD) from *Escherichia coli*. *Biochemistry* 42:7497–7508.
8. Hoffart LM, Barr EW, Guyer RB, Bollinger JM, Jr, Krebs C (2006) A unified mechanism for the α-ketoglutarate-dependent dioxygenases: Evidence for a C-H-cleaving Fe(IV) complex in prolyl-4-hydroxylase. *Proc Natl Acad Sci USA* 103:14738–14743.
9. Price JC, Barr EW, Glass TE, Krebs C, Bollinger JM, Jr (2003) Evidence for hydrogen abstraction from C1 of taurine by the high-spin Fe(IV) intermediate detected during oxygen activation by taurine:α-ketoglutarate dioxygenase (TauD). *J Am Chem Soc* 125:13008–13009.
10. Proshlyakov DA, Henshaw TF, Monterosso GR, Ryle MJ, Hausinger RP (2004) Direct detection of oxygen intermediates in the nonheme Fe enzyme taurine/α-ketoglutarate dioxygenase. *J Am Chem Soc* 126:1022–1023.
11. Riggs-Gelasco PJ, et al. (2004) EXAFS spectroscopic evidence for an Fe=O unit in the Fe(IV) intermediate observed during oxygen activation by taurine:α-ketoglutarate dioxygenase. *J Am Chem Soc* 126:8108–8109.
12. Vaillancourt FH, Yin J, Walsh CT (2005) SyrB2 in syringomycin E biosynthesis is a nonheme Fe^{II} α-ketoglutarate- and O_2-dependent halogenase. *Proc Natl Acad Sci USA* 102:10111–10116.
13. Que L, Jr (2000) One motif—many different reactions. *Nat Struct Biol* 7:182–184.
14. Blasiak LC, Vaillancourt FH, Walsh CT, Drennan CL (2006) Crystal structure of the non-haem iron halogenase SyrB2 in syringomycin biosynthesis. *Nature* 440:368–371.
15. Galonić DP, Barr EW, Walsh CT, Bollinger JM, Jr, Krebs C (2007) Two interconverting Fe(IV) intermediates in aliphatic chlorination by the halogenase CytC3. *Nat Chem Biol* 3:113–116.
16. Matthews ML, et al. (2009) Substrate-triggered formation and remarkable stability of the C-H bond-cleaving chloroferryl intermediate in the aliphatic halogenase, SyrB2. *Biochemistry* 48:4331–4343.
17. Cook GK, Mayer JM (1994) C-H bond activation by metal oxo species: Oxidation of cyclohexane by chromyl chloride. *J Am Chem Soc* 116:1855–1868.
18. Kochi JK (1973) Oxidation-reduction reactions of free radicals and metal complexes. *Free Radicals*, ed Kochi JK (Wiley, New York), Vol 1, pp 591–683.
19. Luo YR (2007) *Comprehensive Handbook of Chemical Bond Energies* (CRC, Boca Raton, FL).
20. Kojima T, Leising RA, Yan S, Que L, Jr (1993) Alkane functionalization at nonheme iron centers. Stoichiometric transfer of metal-bound ligands to alkane. *J Am Chem Soc* 115:11328–11335.
21. de Visser SP, Latifi R (2009) Carbon dioxide: A waste product in the catalytic cycle of alpha-ketoglutarate dependent halogenases prevents the formation of hydroxylated byproducts. *J Phys Chem B* 113:12–14.
22. Pandian S, Vincent MA, Hillier IH, Burton NA (2009) Why does the enzyme SyrB2 chlorinate, but does not hydroxylate, saturated hydrocarbons? A density functional theory (DFT) study. *Dalton Trans*, 6201–6207.
23. Hammes-Schiffer S, Soudackov AV (2008) Proton-coupled electron transfer in solution, proteins, and electrochemistry. *J Phys Chem B* 112:14108–14123.
24. Steenken S, Neta P (1982) Oxidation of substituted alkyl radicals by hexachloroiridate^{2-}, hexacyanoferrate^{3-}, and permanganate ions in aqueous solution. Electron transfer versus chlorine transfer from hexachloroiridate^{2-} ion. *J Am Chem Soc* 104:1244–1248.
25. Al-Sheikhly M, McLaughlin WL (1991) The mechanisms of the reduction reactions of chromium(VI) in the radiolysis of acidic potassium and silver dichromate solutions in the presence or absence of acetic acid. *Radiat Phys Chem* 38:203–211.